Tip-growth of quasi-metallic bilayer graphene nanoribbons with armchair chirality

Shuo Lou[1,2†], Bosai Lyu[1,2†], Jiajun Chen[1,2†], Xianliang Zhou[1,2†], Wenwu Jiang[3,4], Lu Qiu[5,6], Peiyue Shen[1,2], Saiqun Ma[1,2], Zhichun Zhang[1,2], Yufeng Xie[1,2], Zhenghan Wu[1,2], Yi Chen[1,2], Kunqi Xu[1,2], Qi Liang[1,2], Kenji Watanabe[7], Takashi Taniguchi[8], Lede Xian[9,10,11], Guangyu Zhang[11,12,13], Wengen Ouyang[3,4], Feng Ding[5,6,14], Zhiwen Shi[1,2,15*]

[1]Key Laboratory of Artificial Structures and Quantum Control (Ministry of Education), Shenyang National Laboratory for Materials Science, School of Physics and Astronomy, Shanghai Jiao Tong University, Shanghai 200240, China.

[2]Collaborative Innovation Center of Advanced Microstructures, Nanjing University, Nanjing 210093, China.

[3]Department of Engineering Mechanics, School of Civil Engineering, Wuhan University, Wuhan, Hubei 430072, China.

[4]State Key Laboratory of Water Resources and Hydropower Engineering Science, Wuhan University, Wuhan 430072, China

[5]Centre for Multidimensional Carbon Materials, Institute for Basic Science, Ulsan 44919, South Korea.

[6]School of Materials Science and Engineering, Ulsan National Institute of Science and Technology, Ulsan 44919, South Korea

[7]Research Center for Functional Materials, National Institute for Materials Science, 1-1 Namiki, Tsukuba 305-0044, Japan.

[8]International Center for Materials Nanoarchitectonics, National Institute for Materials Science, 1-1 Namiki, Tsukuba 305-0044, Japan.

[9]Songshan Lake Materials Laboratory, Dongguan, Guangdong 523808, China.

[10]Max Planck Institute for the Structure and Dynamics of Matter, Center for Free Electron Laser Science, 22761 Hamburg, Germany.

[11]Hefei National Research Center for Physical Sciences at the Microscale, University of Science and Technology of China, Hefei, Anhui 230026, China.

[12]Beijing National Laboratory for Condensed Matter Physics and Institute of Physics, Chinese

Academy of Sciences, Beijing 100190, China

[13]School of Physical Sciences, University of Chinese Academy of Sciences, Beijing 100190, China

[14]Shenzhen Institute of Advanced Technology, Chinese Academy of Sciences, Shenzhen 518055, China

[15]Tsung-Dao Lee Institute, Shanghai Jiao Tong University, Shanghai, 200240, China.

[†]These authors contributed equally to this work.

*Correspondence to: zwshi@sjtu.edu.cn

1. **Growth condition for the tip-growth GNRs.**
2. **GNRs termination morphology.**
3. **Uniform armchair chirality of GNRs on large range h-BN substrates.**
4. **Long tip-growth GNRs.**
5. **Distribution of diameters of catalyst particles.**
6. **Distribution of GNR widths.**
7. **Distribution of corner angles of the GNRs catalyzed by Fe/Co/Ni nanoparticles, respectively.**
8. **AFM images of GNRs and h-BN crystal directions.**
9. **The relation between orientations of GNRs and h-BN wrinkles.**
10. **Plasmons in the bilayer armchair GNRs.**

1. Growth condition for the tip-growth GNRs.

The growth condition and process are described as follows. Firstly, samples are heated to the growth temperature in a CVD furnace with a flow of mixed Ar and H_2. Then, CH_4 gas is fed in as carbon source for the growth of GNRs. A typical growth duration is 30-40 minutes. Lastly, the samples are cooled down to room temperature with protective gas of Ar and H_2. The pressure during the whole process is atmospheric pressure.

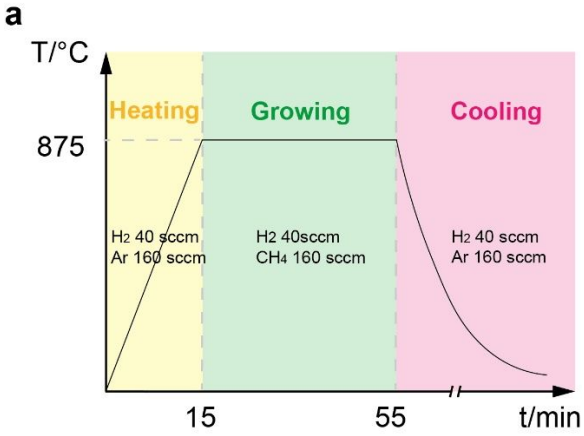

Figure S1. Typical growth condition for tip-growth GNRs catalyzed by Fe/Co/Ni nanoparticles.

2. GNRs termination morphology.

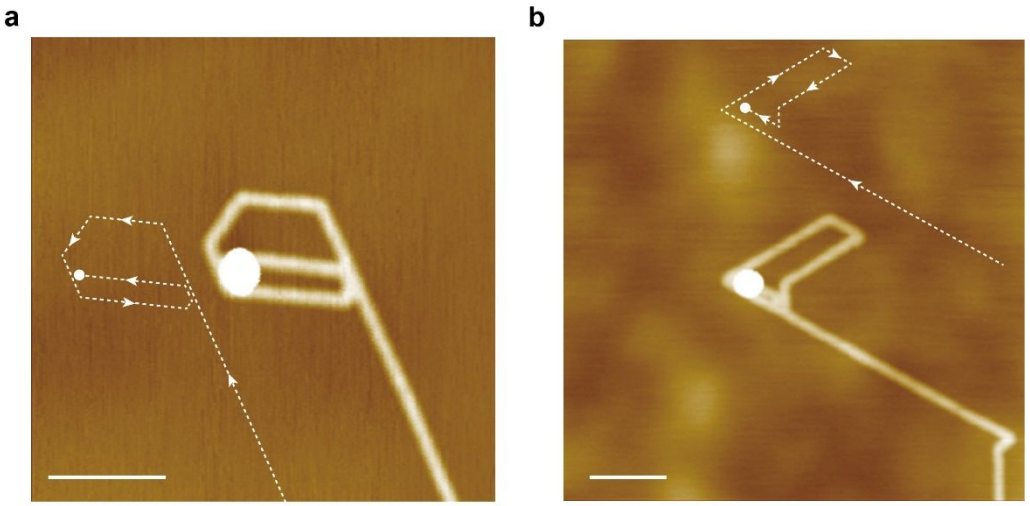

Figure S2. a-b. Common GNRs termination morphology created by the movement of catalysts. A catalyst was trapped in a closed structure formed by the as-grown GNR itself, causing the GNR to stop growing. This suggests that the catalyst moves during the growth process. The dashed line and arrows indicate catalyst nanoparticle's movement route. Scale bars: 100 nm.

3. Uniform armchair chirality of the GNRs on large range h-BN substrates.

AFM images show the relative alignment directions of dozens of GNRs are 0/60/120°, which follows the 3-fold rotational symmetry of the h-BN substrate. . These regular arrangement reveals the single chirality of the as-grown GNRs.

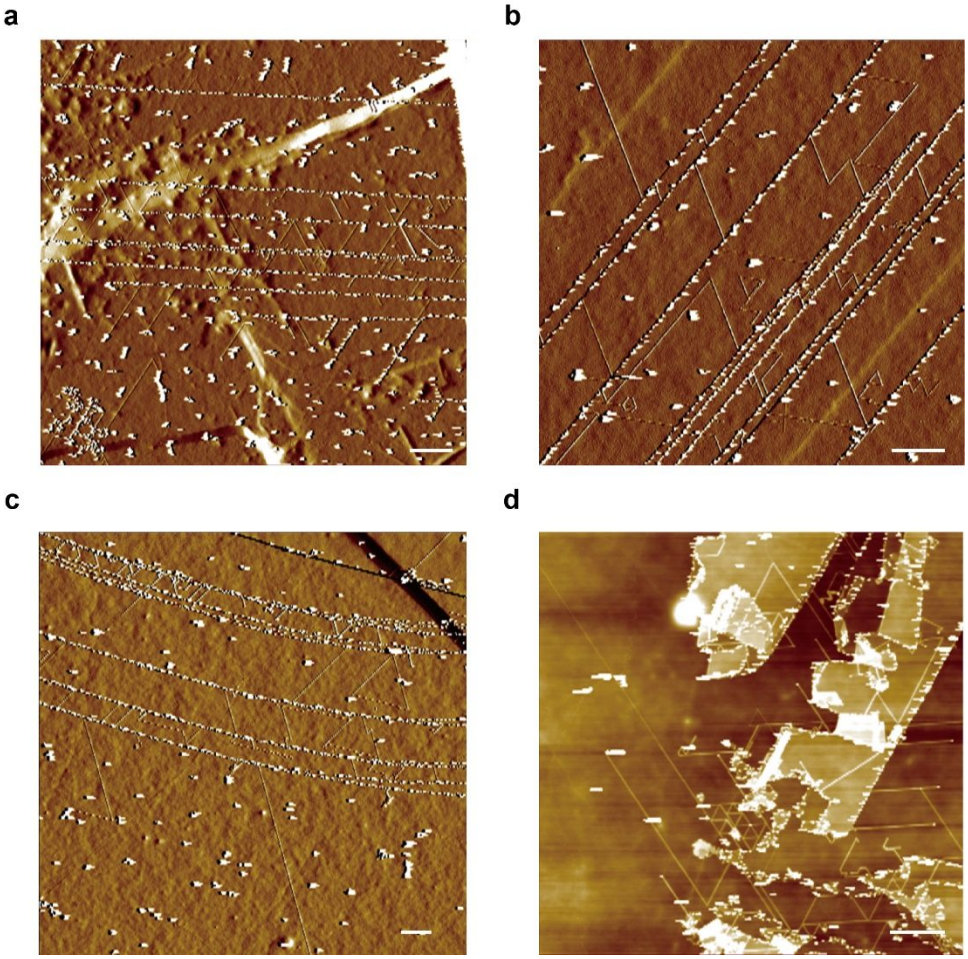

Figure S3. a-d. In large area h-BN substrates, lots of GNRs with armchair chirality are observed, showing the uniformity of the armchair chirality. Scale bar: 1 μm in (a); 500 nm in (b), (c) and (d).

4. Long tip-growth GNRs.

Long GNRs are typically straight. The tip-growth process will be terminated if catalysts are trapped in a closed structure formed by the as-grown GNR itself. Therefore, straight tip-growth GNRs tend to have longer lengths.

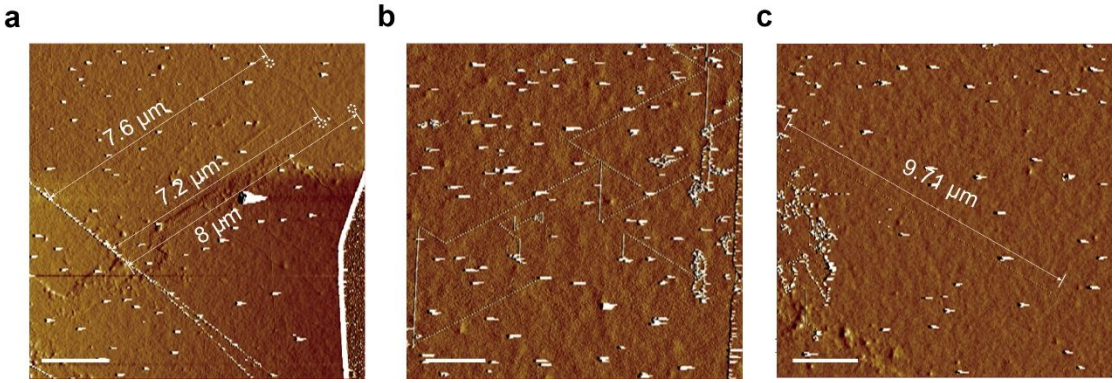

Figure S4. a-c. AFM images of long tip-growth GNRs. **a** and **c,** Straight long tip-growth GNRs with length around 7-9µm. **b**, Long tip-growth GNRs with 60°/120° corner angles. Scale bars: 2µm in (a) and (c); 1µm in (b).

5. Distribution of diameters of catalyst particles.

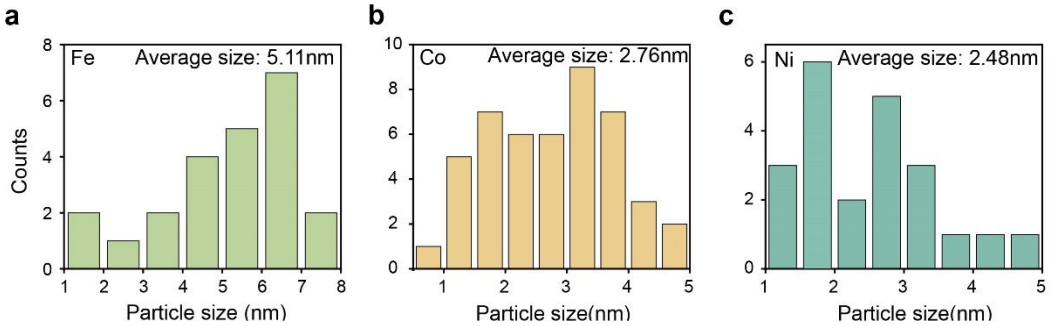

Figure S5. Distribution of catalyst nanoparticle diameters: Fe **(a)**, Co **(b)**, Ni **(c)**. Average diameter of catalyst nanoparticles: Fe 5.11nm, Co 2.76nm, Ni 2.48nm.

6. Distribution of GNR widths.

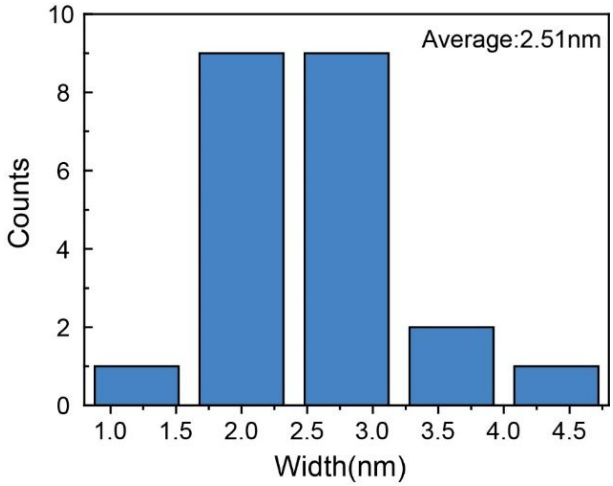

Figure S6. Distribution of GNR widths. The width of GNRs catalyzed by Ni nanoparticles ranges from 1 nm to 5 nm, with an average value of 2.51nm.

7. **Distribution of corner angles of the GNRs catalyzed by Fe/Co/Ni nanoparticles, respectively.**

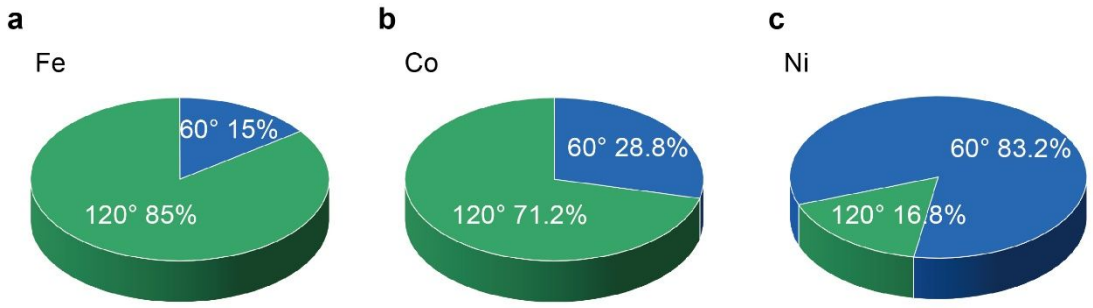

Figure S7. a. 85% corners of GNRs catalyzed by Fe nanoparticle are 120° and 15% corners are 60°. **b.** 71.2% corners of GNRs catalyzed by Co nanoparticle are 120° and 28.8% corners are 60°. **c.** 16.8% corners of GNRs catalyzed by Ni nanoparticle are 120° and 83.2% corners are 60°. The nanoribbons catalyzed by Fe and Co tend to turn at 120°angle, while nanoribbons catalyzed by Ni tend to turn at 60°angle.

8. AFM images of GNRs and h-BN crystal directions.

In addition to the AFM images shown in the main text, we here provide more AFM image of the as-grown GNRs. We also display the fine scanning of the crystal directions of the h-BN substrate. All the GNRs are in the armchair direction of the underneath h-BN substrate.

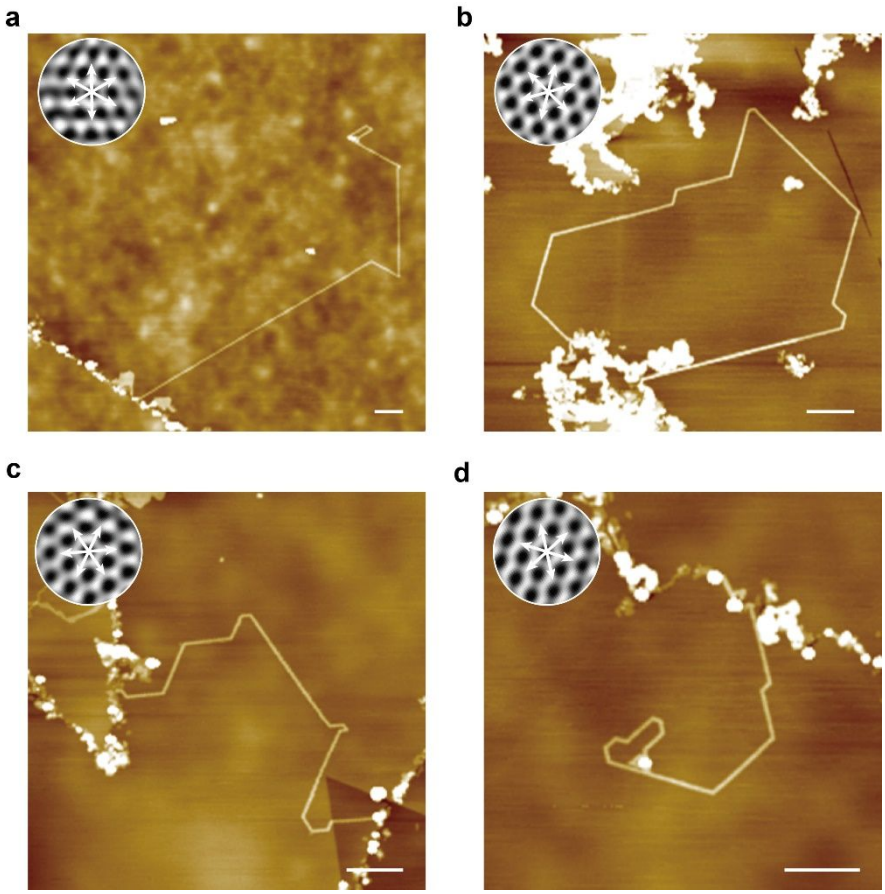

Figure S8. a-d. AFM images of GNRs and beneath h-BN substrate crystal directions. The insets present the high-resolution AFM image of h-BN, showing the crystal structure of the h-BN. Arrows denote armchair directions of the h-BN crystals. Scale bar: 100 nm.

9. The relation between orientations of GNRs and h-BN wrinkles.

The GNRs also parallel with the wrinkles of h-BN, which is known to be in the armchair direction. This provide another evidence that the GNRs are of armchair edge type.

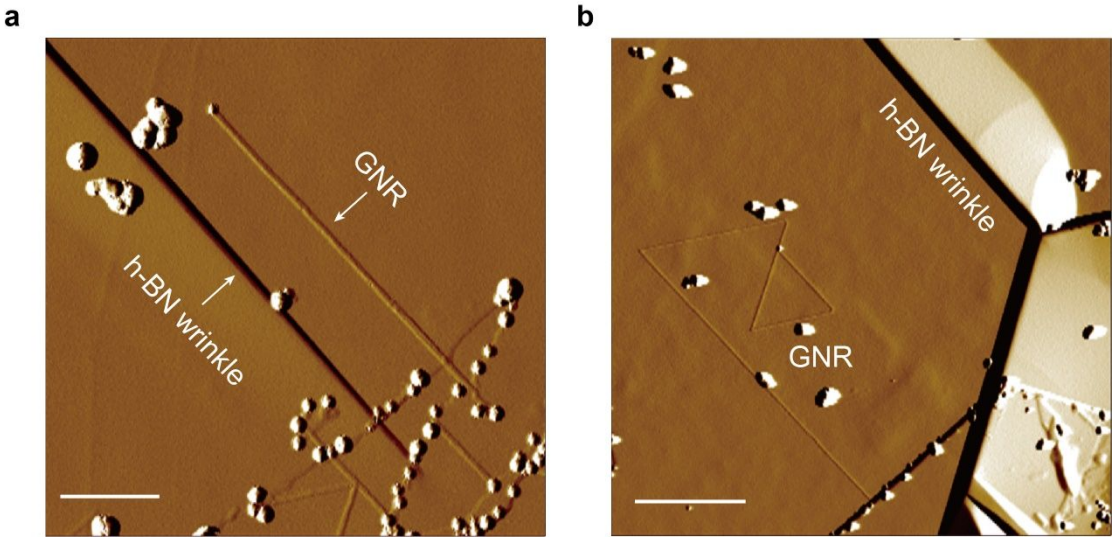

Figure S9. a-b. Tip-growth GNRs are typically parallel with wrinkles of h-BN substrates and h-BN wrinkles are confirmed to follow the armchair directions. This provides one more evidence for the armchair chirality of the GNRs. Scale bars: 1 μm.

10. Plasmons in the bilayer armchair GNRs.

Due to quasi-metallic properties of bilayer GNRs, all these tip-growth mode bilayer GNRs have noticeable plasmon response under scanning near-field optical microscopy (SNOM). The plasmon wavelength of bilayer GNRs ranges from 60nm to 80nm, which is similar to, but slightly smaller than, that of carbon nanotubes (CNTs). One significant difference in SNOM images between GNRs and CNTs is the brightness, with GNRs typically appearing darker than CNTs. This is attributed to the weaker optical conductivity of GNRs in the infrared region compared to nanotubes. The intensity in SNOM images is influenced by the relative amplitude of near-field scattering, which is determined by local optical conductivity. At the far infrared frequency used in SNOM imaging, the optical conductivity of GNRs and CNTs is primarily determined by their free electrons. Metallic CNTs have higher carrier mobilities, resulting in larger optical conductivity than GNRs. Consequently, GNRs exhibit a weaker near-field infrared response than CNTs.

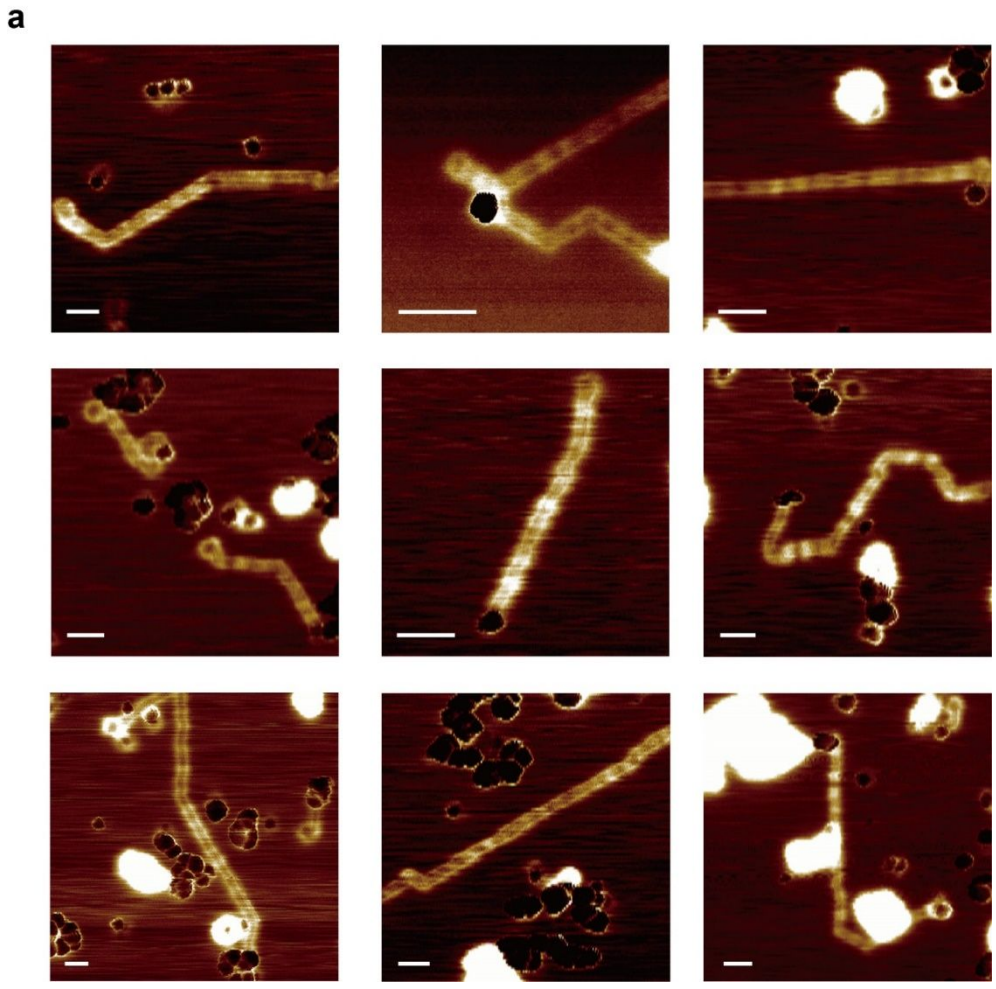

Figure S10. The as-grown bilayer armchair GNRs show notable plasmonic response, reflecting

their metallic nature. A home-built scanning near-field optical microscopy (SNOM) setup (main components include: Innova AFM, Bruker; L3S CO_2 laser, Access Laser; and KLD-0.1-J1 MCT detector, Kolmar) was used to detect the infrared response of the as-grown samples. Infrared beam of 10.6 μm was focused onto the apex of a gold-coated AFM tip (MikroMasch HQ:NSC35/Cr-Au). The near-field at the apex was strongly enhanced by the tapped tip, leading to a strong local interaction of light with material that underneath the tip. The scattered light with local optical information of the sample was collected by an infrared detector. Near-field optical images with spatial resolution better than 20 nm can be achieved with sharp AFM tips. Scale bars: 100 nm.